

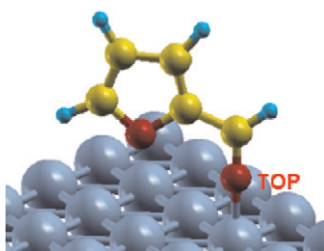


Contents

Kinetics and mechanism of hydrogenation of furfural on Cu/SiO₂ catalysts

pp 1–13

Surapas Sitthisa, Tawan Sooknoi, Yuguang Ma, Perla B. Balbuena, Daniel E. Resasco*

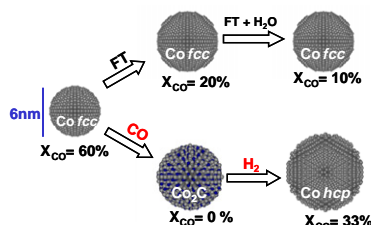


Furfural on a copper surface. The most likely species adsorbed on the Cu surface is a top $\eta^1(\text{O})$ -aldehyde species. Hydrogenation of this species occurs via H attack on the carbonyl C or carbonyl O, resulting in an alkoxide or a hydroxyalkyl intermediate, respectively. DFT calculations indicate that the first attack on the carbonyl O is energetically more favorable.

Structure and catalytic performance of Pt-promoted alumina-supported cobalt catalysts under realistic conditions of Fischer–Tropsch synthesis

pp 14–26

Héline Karaca, Olga V. Safonova*, Stéphane Chambrey, Pascal Fongarland, Pascal Roussel, Anne Griboval-Constant, Maxime Lacroix, Andrei Y. Khodakov*

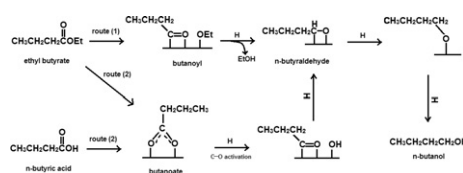


Direct characterization using *in situ* synchrotron-based XRD combined with simultaneous analysis of the reaction products by on-line gas-chromatography was indicative of considerable versatility of alumina-supported cobalt catalysts promoted with platinum under realistic conditions of Fischer–Tropsch synthesis.

Deuterium kinetic isotopic study for hydrogenolysis of ethyl butyrate

pp 27–35

Muthu Kumaran Gnanamani, Gary Jacobs, Robert A. Keogh, Burtron H. Davis*

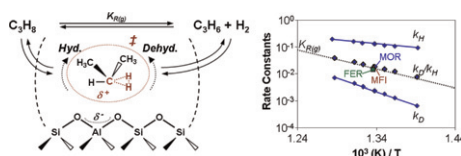


The hydrogenation of ethyl butyrate and *n*-butyric acid to corresponding alcohols follows an inverse kinetic isotope effect on $\gamma\text{-Al}_2\text{O}_3$ -supported cobalt catalyst. Butanoate and butanoyl are the stable surface intermediate species formed over the surface of catalyst, and hydrogenation of these intermediates is likely involved in the rate-limiting step.

Catalytic hydrogenation of alkenes on acidic zeolites: Mechanistic connections to monomolecular alkane dehydrogenation reactions

pp 36–45

Rajamani Gounder, Enrique Iglesia*

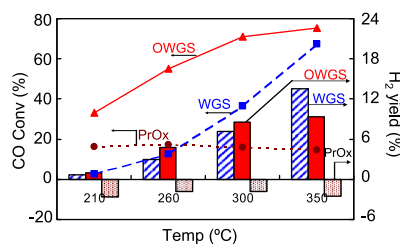


Alkene Hydrogenation on Acidic Zeolites: Brønsted acid sites in FER, MFI, and MOR zeolites catalyze monomolecular alkane dehydrogenation and its microscopic reverse, alkene hydrogenation with H_2 , via the same kinetically-relevant $(C-H-H)^+$ carbonium-ion-like transition states, even far from equilibrium. The measured rate constants, activation energies and activation entropies for dehydrogenation and hydrogenation are related by the equilibrium constant and the enthalpy and entropy for the stoichiometric gas-phase reaction, which are independent of the reactivity and structure of the active sites.

Oxygen-enhanced water gas shift on ceria-supported Pd–Cu and Pt–Cu bimetallic catalysts

pp 46–53

Junichiro Kugai, Jeffrey T. Miller, Neng Guo, Chunshan Song*

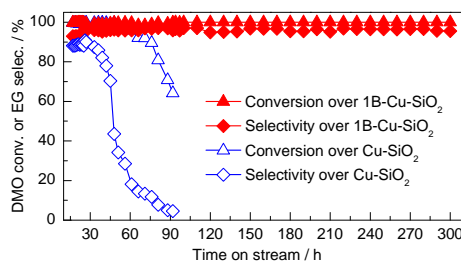


Oxygen-enhanced water gas shift (OWGS) can lead to much higher CO conversion and higher H_2 yield than the conventional water gas shift (WGS) over the same bimetallic Pt–Cu/CeO₂ catalyst under comparable reaction conditions.

Effect of boric oxide doping on the stability and activity of a Cu–SiO₂ catalyst for vapor-phase hydrogenation of dimethyl oxalate to ethylene glycol

pp 54–63

Zhe He, Haiqiang Lin, Ping He, Youzhu Yuan*

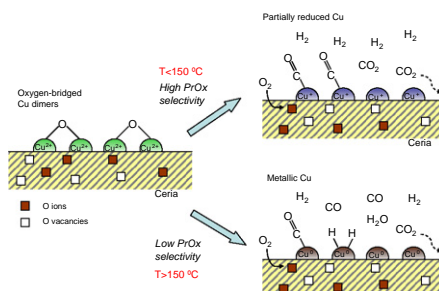


Doping a proper quantity of boric oxide onto a Cu–SiO₂ catalyst significantly improves its stability as well as its activity for the vapor-phase hydrogenation of dimethyl oxalate to ethylene glycol.

Temperature-induced evolution of reaction sites and mechanisms during preferential oxidation of CO

pp 64–71

Richard Kydd, Davide Ferri*, Paul Hug, Jason Scott, Wey Yang Teoh*, Rose Amal

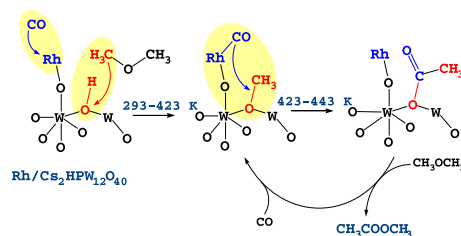


The origin of preferential oxidation (PROX) of CO in the presence of H_2 was traced to the carbonyl stabilization on partially-reduced copper oxide surface, at below 150 °C, preventing thus incoming H_2 from approaching the oxidation sites.

Carbonylation of dimethyl ether on solid Rh-promoted Cs-salt of Keggin 12-H₃PW₁₂O₄₀: A solid-state NMR study of the reaction mechanism

pp 72–79

Mikhail V. Luzgin, Maxim S. Kazantsev, Galina G. Volkova, Wei Wang, Alexander G. Stepanov*

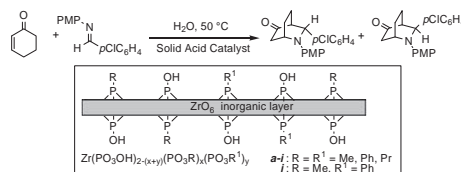


The mechanism of the halide-free carbonylation of dimethyl ether with carbon monoxide on Rh/Cs₂HPW₁₂O₄₀ has been established. The formation and inter-conversions of the reaction intermediates – surface methoxy-groups, Rh-carbonyls and surface acetates, has been monitored with ¹³C solid-state NMR. The bi-functional character of the catalyst has been directly demonstrated.

New zirconium hydrogen phosphate alkyl and/or aryl phosphonates with high surface area as heterogeneous Brønsted acid catalysts for aza-Diels–Alder reaction in aqueous medium

pp 80–87

Daniela Lanari, Francesca Montanari, Fabio Marmottini, Oriana Piermatti*, Mara Orrù, Luigi Vaccaro

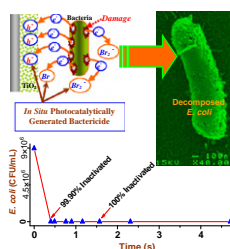


New zirconium hydrogen phosphate alkyl and/or aryl phosphonates with high surface area (200–380 m²/g) have been prepared, and their Brønsted acid catalytic activity was tested on the direct aza-Diels–Alder reaction of 2-cyclohexen-1-one with N-PMP-pCl-benzaldimine in aqueous medium.

In situ photoelectrocatalytic generation of bactericide for instant inactivation and rapid decomposition of Gram-negative bacteria

pp 88–94

Guiying Li, Xiaolu Liu, Haimin Zhang, Taicheng An*, Shanqing Zhang, Anthony R. Carroll, Huijun Zhao*

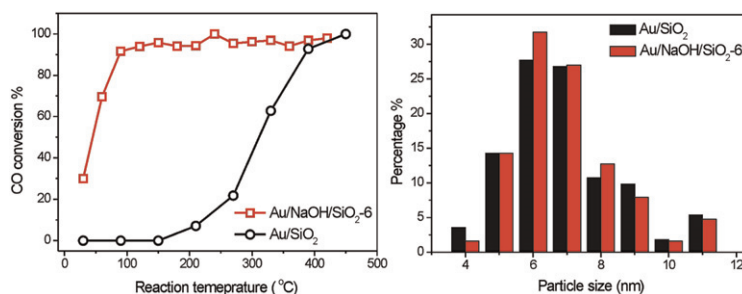


The proposed bactericidal method utilizes *in situ* photoelectrocatalytically generated bactericides to achieve instant inactivation and rapid decomposition of Gram-negative bacteria. The method is capable of inactivating 99.90% of *Escherichia coli* within 0.4 s and mineralizing over 40% biomass within 600 s.

Hydroxyls-induced oxygen activation on “inert” Au nanoparticles for low-temperature CO oxidation

pp 95–103

Kun Qian, Wenhua Zhang, Huaxing Sun, Jun Fang, Bo He, Yunsheng Ma, Zhiqian Jiang, Shiqiang Wei, Jinlong Yang*, Weixin Huang*

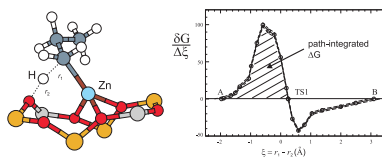


Hydroxyls can induce the activation of molecular oxygen on “inert” Au nanoparticles for low-temperature CO oxidation.

Dehydrogenation of propane over Zn–MOR. Static and dynamic reaction energy diagram

pp 104–116

L. Benco*, T. Bucko, J. Hafner

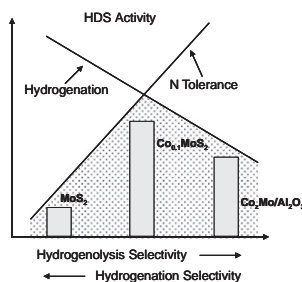


Configuration of propane adsorbed on the Zn²⁺ cation used for the dissociation of the hydrogen atom (left). Gradients of the free energy calculated for the dissociation along the reaction path (right).

Ultra-deep hydrodesulfurization on MoS₂ and Co_{0.1}MoS₂: Intrinsic vs. environmental factors

pp 117–122

Teh C. Ho*, Jonathan M. McConnachie

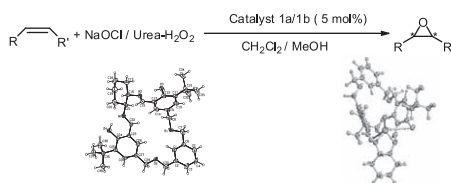


An ultra-deep diesel hydrodesulfurization catalyst such as the unsupported Co_{0.1}MoS₂ requires a balance between the hydrogenation function and resilience to organonitrogen inhibition. The Al₂O₃-supported Co₂Mo catalyst ($z > 0.3$) is a commercial hydrodesulfurization catalyst.

Chiral macrocyclic salen Mn(III) complexes catalyzed enantioselective epoxidation of non-functionalized alkenes using NaOCl and urea H₂O₂ as oxidants

pp 123–127

Nabin Ch. Maity, Sayed H.R. Abdi*, Rukhsana I. Kureshy, Noor-ul H. Khan, E. Suresh, Ganga P. Dangi, Hari C. Bajaj



Chiral macrocyclic Mn(III) Schiff base complexes catalyze the enantioselective epoxidation of non-functionalized alkenes with sodium hypochlorite or urea hydrogen peroxide in presence of several pyridine *N*-oxide at 0–5 °C.